

Cite this: *Soft Matter*, 2011, **7**, 7511

www.rsc.org/softmatter

PAPER

## Reversible white-light actuation of carbon nanotube incorporated liquid crystalline elastomer nanocomposites†

Chensha Li,<sup>‡a</sup> Ye Liu,<sup>‡a</sup> Chi-wei Lo<sup>b</sup> and Hongrui Jiang<sup>\*ab</sup>

Received 28th April 2011, Accepted 31st May 2011

DOI: 10.1039/c1sm05776f

We present single-wall carbon nanotube (SWCNT) incorporated liquid crystal elastomer (LCE) nanocomposites that demonstrate strong, reversible photoactuation. The matrix nematic LCE material possesses reversible thermal deformation, while SWCNTs perform photothermal energy conversion and local heat dissipation upon irradiation. The resultant SWCNT–LCE nanocomposites exhibit effective photoactuation not only by infrared (IR) irradiation, but also white light with an intensity on the order of 100 mW cm<sup>-2</sup>. Rapid and reversible photo-induced strain was observed. The nanocomposite films contracted up to one third of the original length in several seconds under the irradiation of white light, and recovered to the original length in several seconds after the light source was switched off. Moreover, the nematic–isotropic transition temperatures of the SWCNT–LCE nanocomposites were evidently lower than that of the blank LCE by up to 19 °C.

### Introduction

Certain materials that can change their dimensions and shapes upon application of a given stimulus, such as heat and light, have been of great interest.<sup>1</sup> Shape-memory alloys<sup>2</sup> or polymers<sup>3</sup> are good examples of such smart actuation materials. However, in most cases a shape-memory system is not reversible, requiring a reset after the actuation. Nematic liquid crystal elastomers (LCEs)<sup>4</sup> have proven to be a truly equilibrium reversible actuating system which can return to the equilibrium shape once the stimulus is removed. They possess several important features that lead to promising new actuation materials,<sup>5–11</sup> such as orientational order exhibited by the mesogenic units in amorphous soft materials, topological constraints *via* the crosslinks, and responsive molecular shape due to the coupling between the orientational order and mechanical strain.<sup>4</sup> Nematic LCEs can dramatically and reversibly contract or elongate in response to temperature change. However, the response to an external stimulus is generally slow due to the low energy-transfer ability and thermal-conductivity, thus being difficult to be actuated remotely and limiting their potential applications.

The response of a polymer to an external stimulus can be modified and improved when incorporated with different materials that impart new physical response. Carbon nanotubes (CNTs) are one of the effective filling materials for nanocomposites due to their one-dimension structures, nanometre-scale diameters, high aspect ratios, large surface areas, and excellent conductivities and other physical and mechanical properties.<sup>12–14</sup> CNTs, especially the single-wall carbon nanotubes (SWCNTs), show strong absorptions in the visible and near-IR region owing to band gap transitions.<sup>15</sup> They can efficiently absorb and convert photoenergy into thermal energy, and serve as a nanoscale heat source and thermal conduction pathway to heat the matrices effectively. Hence, SWCNTs can offer superior opportunities for the photoactuation of thermal responsive materials. Studies showed that the shape-memory behavior of CNT–polyurethane nanocomposites irradiated *via* infrared (IR) light is more sensitive compared to the simplex polyurethane material.<sup>16</sup> It was also recently reported that LCEs incorporated with CNTs can be significantly actuated by IR irradiation.<sup>17,18</sup>

In this work, we prepared LCE nanocomposites using SWCNTs as a filler in a nematic side-chain LCE matrix with polysiloxane backbones. LCE nanocomposites with high loading level of SWCNTs up to 1.8 wt% were made by a relatively simple method. Experimental results showed that the addition of SWCNTs into the LCE matrix evidently lowered the material's nematic–isotropic transition temperature ( $T_{ni}$ ) by up to about 19 °C, from 82 °C to about 63 °C. The decrease in  $T_{ni}$  of LCE due to incorporating SWCNTs was much larger than previously reported.<sup>18</sup> Moreover, we demonstrated that the SWCNT–LCE nanocomposites could be reversibly and rapidly actuated by

<sup>a</sup>Department of Electrical and Computer Engineering, University of Wisconsin-Madison, WI, 53706, USA. E-mail: hongrui@engr.wisc.edu; Tel: +1(608)-265-9418

<sup>b</sup>Materials Science Program, University of Wisconsin-Madison, WI, 53706, USA

† Electronic supplementary information (ESI) available: On-line supplementary information includes schematics of MBB and 11UB, a video showing the photoactuation of the films, and discussion on film fabrication. See DOI: 10.1039/c1sm05776f

‡ These authors contributed equally to this work.

white light from a wide-spectrum light source, rather than limited to IR or other specific wavelength as previously reported.

## Experimental

### The synthesis of the compounds

The pendant mesogenic group, 4-methoxyphenyl-4-(1-buteneoxy) benzoate (MBB), and di-functional crosslinking group, 1,4-alkeneoxybenzene (11UB), were synthesized as follows by leveraging the work reported in literature, ref. 19 and 20 (see Scheme S1 in the ESI†).

**Synthesis of 4-methoxyphenyl-4-(1-buteneoxy) benzoate (MBB).** A solution of but-3-en-1-ol (6.2 g, 86 mmol), 4-hydroxybenzoic acid ethyl ester (14.3 g, 86 mmol) and triphenyl phosphine (22.56 g, 86 mmol) in tetrahydrofuran (40 mL) was added with diethyl azo dicarboxylate (13.54 mL, 14.98 g, 86 mmol) in drops over 30 minutes at the room temperature under an anhydrous nitrogen atmosphere. The reaction mixture was stirred for 24 hours and the solvent was removed in vacuum. The product was purified by flash column chromatography using silica gel as the stationary phase and the mixture of hexane and dichloromethane, with a ratio of 4 : 1, as the eluent. The solvent was removed in vacuum to yield 4-but-3-enyloxy-benzoic acid ethyl ester (13.4 g, 61 mmol, yield ratio: 71%) as a slightly yellow oil. A solution of 4-but-3-enyloxy-benzoic acid ethyl ester (7.8 g, 35.4 mmol), sodium hydroxide (3 g, 75 mmol) in ethanol (100 mL) and water (100 mL) was heated under reflux for 10 hours. The reaction mixture was cooled to the room temperature and acidified to pH 2 by hydrochloric acid. The white precipitate was collected and purified by washing with water. The product was recrystallized from ethanol to give 4-but-3-enyloxy-benzoic acid as a white solid (6.5 g, 33.8 mmol, yield ratio: 97%, mp = 116 °C). A mixture of 4-but-3-enyloxy-benzoic acid (1.89 g, 9.84 mmol), 4-methoxy phenol (1.2216 g, 9.84 mmol), 4-dimethylaminopyridine (1.2022 g, 9.84 mmol), 1,3-diisopropylcarbodiimide (1.4654 g, 11.6 mmol) and *para*-toluene sulfonic acid (1.8718 g, 9.84 mmol) in dry dichloromethane (20 mL) was stirred at the room temperature for 12 hours. The solvent was removed in vacuum and the resultant white solid was purified by flash column chromatography using silica gel as the stationary phase and dichloromethane as the eluant to give MBB. The product was recrystallized from ethanol (2.00 g, 6.7 mmol, yield ratio: 69%, mp = 79 °C) as white crystals. <sup>1</sup>H NMR (ppm rel. to TMS): 2.55 (dt, 2H, =CHCH<sub>2</sub>, *J* = 6.7), 3.82 (s, 3H, OCH<sub>3</sub>), 4.09 (t, 3H, =CHCH<sub>2</sub>CH<sub>3</sub>, *J* = 6.7), 5.14 (dd, 1H, CH= *trans* to R, *J* = 10.3, 1.3), 5.19 (dd, 1H, CH= *cis* to R, *J* = 17.2, 1.6), 5.91 (m, 1H, CH=CH<sub>2</sub>, *J* = 6.7–17.1), 6.92 (d, 2H, 2 aromatic H *ortho* to OCH<sub>3</sub>, *J* = 9.0), 6.96 (d, 2H, 2 aromatic H *ortho* to OR', *J* = 8.9), 7.11 (d, 2H, 2 aromatic H *meta* to OCH<sub>3</sub>, *J* = 9.0), 8.13 (d, 2 aromatic H *meta* to OR', *J* = 8.9).

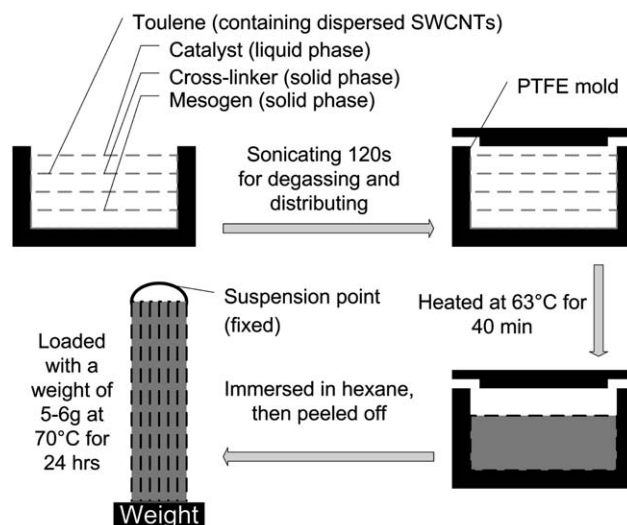
**Synthesis of 1,4-alkeneoxybenzene (11UB).** A solution of hydroquinone (5.5 g, 50 mmol) and potassium carbonate (24.2 g, 175 mmol) in 100 mL ethanol was heated under reflux. A solution of 11-chloro-1-undecene (22.65 g, 120 mmol) in ethanol (250 mL) was then added in drops to this over 30 minutes. After 18 hours of continued heating under reflux, the reaction mixture

was poured into 1000 mL of iced water. This solution was extracted three times with diethyl ether (2000 mL in total). The organic layer was washed twice with saturated aqueous solution of sodium carbonate (500 mL in total) and once with water (500 mL), followed by drying over anhydrous magnesium sulfate. The diethyl ether was removed in vacuum, and the precipitation was subsequently purified by flash column chromatography using silica gel as the stationary phase and a mixture of dichloromethane and hexane, with the ratio of 1 : 3, as the eluent, followed by solvent removal in vacuum to yield 11UB as a white solid. The product was recrystallized from ethanol (30.1 g, yield ratio: 65%, mp = 56 °C). <sup>1</sup>H NMR (ppm rel. to TMS): 1.18 (m, 12H, O(CH<sub>2</sub>)<sub>2</sub>C<sub>6</sub>H<sub>12</sub>, *J* = 7), 1.73 (qn, 2H, CH<sub>2</sub> CH<sub>2</sub>, *J* = 6.5–7.0 Hz), 2.03 (dt, 2H, =CHCH<sub>2</sub>, *J* = 6.5–7.0 Hz), 3.88 (t, 2H, OCH<sub>2</sub>, *J* = 6.6 Hz), 4.92 (dd, 1H, CH= *trans* to R, *J* = 6.9, 1.1), 4.98 (dd, CH= *cis* to R, 1H, *J* = 13.0, 2.1), 5.80 (m, 1H, =CH, *J* = 6.8–3.2), 6.80 (s, 1H, aromatic H).

### Material preparation

The pendant mesogenic group, MBB and 11UB were first synthesized as above. The polymer backbone was a poly-dimethylhydrosiloxane (PMHS) with approximately 60 Si–H units per chain, obtained from ACROS Chemicals (Belgium, USA). The commercial platinum catalyst dichloro(1,5-cyclooctadiene) platinum(II), obtained from Aldrich (St Louis, USA), was solved in toluene.

The side-chain nematic LCE networks with the polysiloxane backbone, aligned in the uniaxial orientation, were prepared by leveraging the procedure reported in ref. 4 and 5. The polysiloxane backbone (PMHS) had its Si–H bonds reacted, using platinum acid catalyst, with the terminal vinyl groups of the mesogenic rod-like molecule (MBB) and the two-functional crosslinker (11UB) by hydrosilation, with a molar ratio of 20 : 1, thus achieving the 10 : 1 ratio of substituted groups on each chain or the effective 9% cross-linking density. The synthesis procedure was through two-stage crosslinking coupled with a drawing process.



**Scheme 1** Fabrication process of SWCNT–LCE nanocomposite films.

The fabrication process of the SWCNT–LCE nanocomposite films is shown in Scheme 1. SWCNTs were mixed into the reaction mixture solution, which was 0.12 g of PMHS, 0.5 g of MBB (1.68 mmol) and 0.068 g of 11UB (0.165 mmol) solved in 2 mL of toluene, under ultrasonication to ensure homogeneous dispersion; the ultrasonic mixing was performed for about 2 min. 100  $\mu$ L of catalyst solution was added into the reaction mixture solution containing SWCNTs; then the solution was cast into a polytetrafluoroethylene (PTFE) rectangular parallel-piped mold with dimensions of 8 cm  $\times$  1 cm  $\times$  1 cm. The mold was first high-power ultrasonicated for 3 minutes to remove the tiny bubbles entrapped in the mixture (this step was necessary, or the fabricated LCE would contain plenty of defects), then heated in an oven at 63  $^{\circ}$ C for 40 min for partial crosslinking process (first crosslinking stage). Thereafter the mold was cooled to the room temperature. The elastomer was then carefully removed from the mold, dried, and slowly uniaxially stretched along the length under a load—it can generally be stretched to 30% to 40% to attain a stable length—to obtain nematic alignment (drawing process). Then the film with the load was heated at 70  $^{\circ}$ C overnight to complete the crosslinking reaction in nematic phase (second crosslinking stage). We prepared SWCNT–LCE samples with SWCNT contents of 0.1, 0.3, 0.7, 1, and 1.8 wt% respectively. The blank nematic LCE was prepared by the same procedure but without SWCNTs. More discussion on the fabrication process can be found in the ESI†.

### Characterization methods

The phase transformation behavior was investigated by differential scanning calorimetry (DSC) measurements (TA Instruments Q100 modulated differential scanning calorimeter, New Castle, DE) at a heating and cooling rate of 10 K  $\text{min}^{-1}$ . The distribution of SWCNTs in the LCE matrix was examined with scanning electron microscopy (SEM; Zeiss LEO 1530, Thornwood, NY). The SWCNT–LCE nanocomposite was broken, and the cross-section was observed with SEM. The LCE mesomorphic properties were observed using polarizing optical microscopy (Nikon Instruments, SMZ 1500, Melville, NY). The photoactuation measurements of the LCE nanocomposite films were performed by using a wide spectrum light source (New Port,

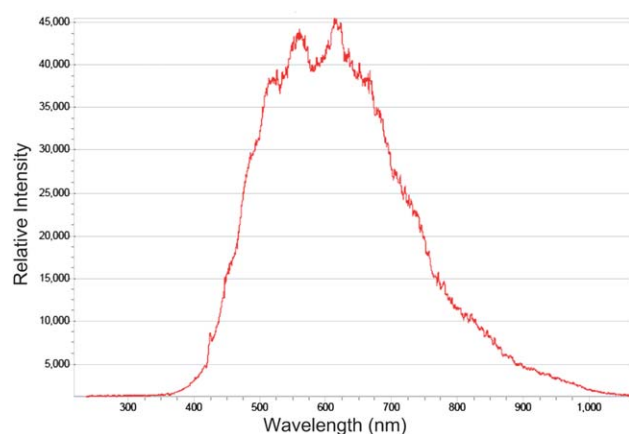


**Fig. 1** The light spectrum emitted by the wide spectrum light source used in the experiments.

Oriel Productline, Model 66885, Irvine, CA). The measured spectrum of its emitted light is shown in Fig. 1. The white light source illuminated the samples with irradiation intensities on the order of 100  $\text{mW cm}^{-2}$ .

The measurements of the actuation of the LCE and LCE nanocomposite films under IR irradiation were performed by using an IR source (Hotspot, Model H. S. 250.3, *F*R, Cheltenham, PA).

The temperature change of the blank LCE film and the SWCNT–LCE films in response to the light stimulus was tested by a multilogger thermometer (HH 506 RA, OMEGA Engineering, Stamford, CT). The detector, with the dimension of 2 mm in length and 100  $\mu$ m in diameter, was placed on the sample surfaces.

The contraction stresses of the films under light irradiation and their tensile strength were measured with a stress meter.

All data reported in this paper were taken at a room temperature of 25  $^{\circ}$ C.

### Results and discussion

The anisotropic alignment of the mesogens in the LCE matrix was evaluated at the room temperature by measuring the transmittance of a probe light through two crossed polarizers with a film between them. The polarizing optical micrographs (POMs) of a blank LCE film and an SWCNT–LCE nanocomposite film are shown in Fig. 2. The highest transmittance appeared when the angle between the stretch direction of the films and the

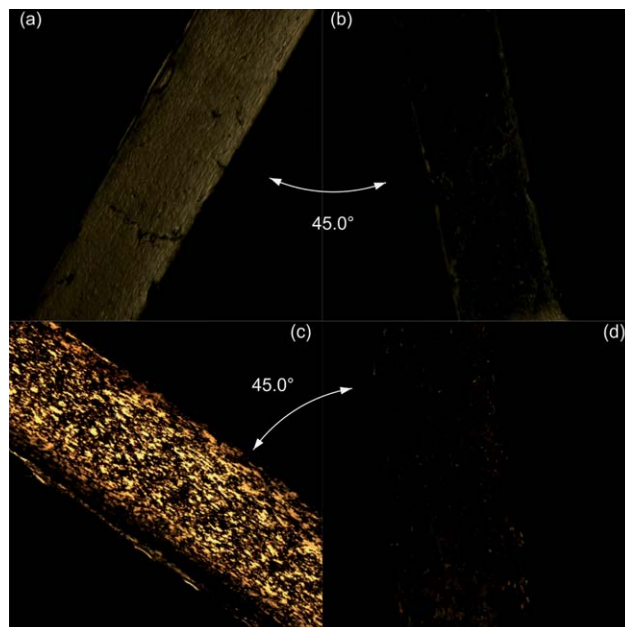


**Fig. 2** POMs of a blank LCE film and an SWCNT–LCE nanocomposite film (0.3 wt% of SWCNT content). (a) The angle between the stretch direction of the blank LCE film and the polarization direction of either polarizer is 45 $^{\circ}$ . (b) The stretch direction of the blank LCE film is parallel to one of the polarization directions. (c) The angle between the stretch direction of the SWCNT–LCE nanocomposite film and the polarization direction of either polarizer is 45 $^{\circ}$ . (d) The stretch direction of the SWCNT–LCE nanocomposite film is parallel to one of the polarization directions.

polarization direction of either polarizer was  $45^\circ$ , while the lowest appeared when the stretch direction was parallel to one of the polarization directions. Periodic changes of dark and bright images were observed by rotating the films with an interval of  $45^\circ$ . The POM observations of the blank LCE film and the SWCNT–LCE nanocomposite film exhibited consistent result, though due to the blocking of light by SWCNTs, the transmittances in the images of the SWCNT–LCE nanocomposite film were much darker. The result proved an LCE nematic-phase texture, and that the mesogenic units were well aligned along the stretch direction. SEM images of the SWCNT–LCE nanocomposites proved that the SWCNTs were effectively dispersed in the LCE matrix, as shown in Fig. 3.

Experiments indicated that these LCE and LCE nanocomposite films contracted along the axis when heated, and regained their original length after cooling down, as shown in Fig. 4. Fully reversible contraction and restoration were observed under these heating/cooling cycles. This shape deformation was induced by the change in the nematic order. Nematic LCE possesses the uniaxial orientational order. The order is characterized by its principal axis, which is the nematic director, and the scalar order parameter which measures the mean orientation of the mesogenic groups with respect to the director. Owing to such internal degree of freedom coupled to the elastic body constituted by rigid rod-like mesogens linked to the chain conformation, the relative movement of crosslinking points provides elastic strains and forces, while the director rotation causes local torques and couple-stresses, which are both intricately connected in the overall macroscopic response of the body. The change in the degree of alignment of mesogenic rods leads to spontaneous elongation or contraction of the whole network along the nematic director. When the nematic LCE is heated above or cooled down below its  $T_{ni}$ , the nematic order is changed, and the spontaneous uniaxial contraction/restoration of the nematic LCE along the director axis can be realized.<sup>4,21</sup>

Fig. 5 presents the DSC measurement of phase transformations in the prepared LCE and SWCNT–LCE nanocomposites. The glass transition temperature ( $T_g$ ) and  $T_{ni}$  measured from the DSC heating cycles are listed in Table 1. It shows that  $T_g$  of all samples are near  $0^\circ\text{C}$ . Therefore, they maintain the elastic property at normal temperatures.  $T_{ni}$  of blank nematic LCE is about  $82^\circ\text{C}$ , while those of the SWCNT–LCE nanocomposites are evidently lower. In general, the higher the SWCNT contents, the lower the  $T_{ni}$ . With 1.8 wt% of SWCNTs,  $T_{ni}$  is as low as about  $63^\circ\text{C}$ . We believe that the mechanism might lie in the thermal–mechanical response of CNTs in the polymer matrices.<sup>16,22</sup> Such thermal stress of CNTs

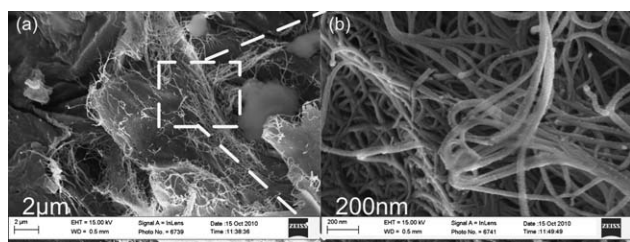


**Fig. 3** SEM image of SWCNTs in the LCE matrix. The SWCNT content in this nanocomposite film is 0.3 wt%.

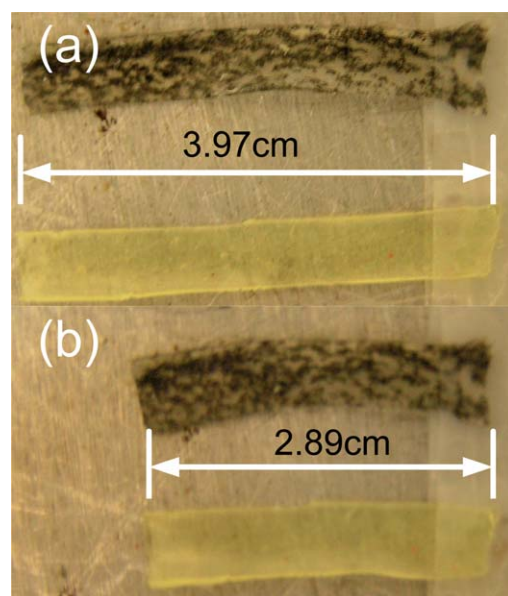


**Fig. 4** Optical images of the thermal actuation of a blank LCE film and an SWCNT–LCE nanocomposite (SWCNT content: 0.3 wt%) film on a hot plate. The films have a dimension of  $4\text{ cm} \times 0.5\text{ cm} \times 0.7\text{ mm}$ . (a) The state of the films when the temperature of the hot plate is  $25^\circ\text{C}$ . (b) The state of the films when the temperature of the hot plate is  $85^\circ\text{C}$ .

might have promoted the transition of the mesogenic groups from the nematic state to the isotropic state, leading to the lowering of  $T_{ni}$ .

Experiments also demonstrated attractive photo-induced actuation characteristics of the SWCNT–LCE nanocomposites (see the video in the ESI<sup>†</sup>). We used a white light source, without filtering to any specific wavelength. Fig. 6 shows the response of a blank LCE film and an SWCNT–LCE nanocomposite film under a white-light irradiation of  $230\text{ mW cm}^{-2}$  in intensity. The blank LCE film, which was essentially phototransparent with a low photothermal energy conversion efficiency, remained unaffected and did not contract. Our experiment further showed that the blank LCE film could not be actuated even under a 10 W

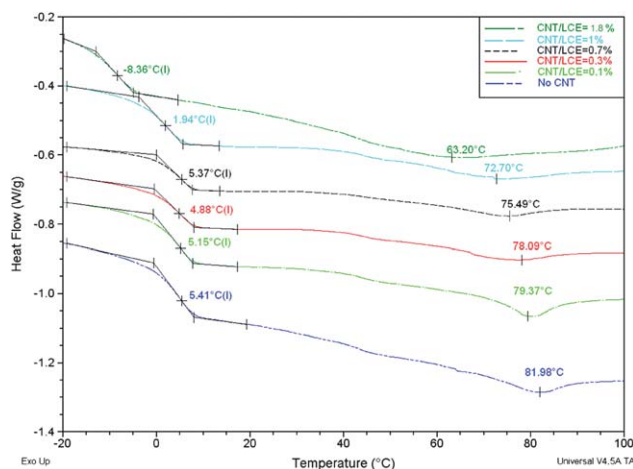


**Fig. 5** DSC data curves of the blank LCE and different SWCNT–LCE nanocomposites.

**Table 1** Characteristics of the blank LCE and SWCNT–LCE nanocomposites. The maximum axial contraction ratios actuated by a photoirradiation is defined as  $(L_0 - L)/L_0$ , where  $L_0$  is the initial length, and  $L_0 - L$  is the maximum stable axial contraction strain under the photoirradiation. The SWCNT–LCE nanocomposites are actuated by white light, while the blank LCE is actuated by IR light. The films have a dimension of  $4\text{ cm} \times 0.5\text{ cm} \times 0.7\text{ mm}$ , and are loaded by 3 g of weights during the photoactuation process.<sup>24</sup>

Samples	$T_g/^\circ\text{C}$	$T_{ni}/^\circ\text{C}$	$(L_0 - L)/L_0$
Blank LCE	5.41	81.98	32.9%
LCE 0.1 wt% SWCNTs	5.15	79.37	35.1%
LCE 0.3 wt% SWCNTs	4.88	78.09	34.8%
LCE 0.7 wt% SWCNTs	5.37	75.49	33.2%
LCE 1 wt% SWCNTs	1.94	72.70	32.1%
LCE 1.8 wt% SWCNTs	-8.36	63.2	29.5%

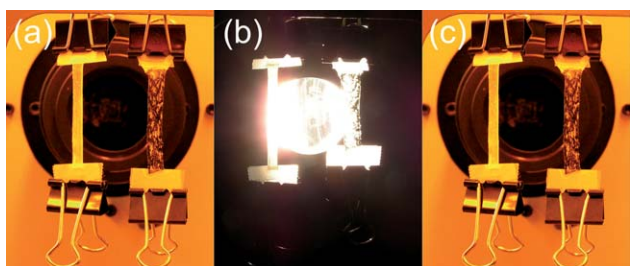


**Fig. 6** Optical images of the photoactuation of blank LCE and SWCNT–LCE nanocomposite (SWCNT content: 0.3 wt%) films. The films have a dimension of  $4\text{ cm} \times 0.5\text{ cm} \times 0.7\text{ mm}$ . They are loaded by 3 g of weights during the photoactuation process. The irradiation intensity here is  $230\text{ mW cm}^{-2}$ . (a) The initial state of the blank LCE and SWCNT–LCE nanocomposite films. (b) Comparison of the two films under irradiation. The blank LCE does not deform after being illuminated for several minutes. In contrast, SWCNT–LCE nanocomposite film starts conspicuous contraction after  $\sim 5$  seconds, and reaches the stable length, which is about  $2/3$  of the initial length, after  $\sim 10$  seconds. (c) The SWCNT–LCE nanocomposite film recovers to its initial length  $\sim 9$  seconds after the light source is switched off.

$\text{cm}^{-2}$  intensity of white-light irradiation (maximum output from our light source). In contrast, the SWCNT–LCE nanocomposite film started conspicuous contraction  $\sim 5$  seconds after being exposed to  $230\text{ mW cm}^{-2}$  of irradiation and reached maximum contraction after  $\sim 10$  seconds, as demonstrated in Fig. 6. It recovered to its initial length  $\sim 9$  seconds after the light source was switched off, indicating completely reversible photoactuation. In addition, experiment indicated that under an irradiation of  $413\text{ mW cm}^{-2}$ , a contraction stress of 75 kPa was created in the SWCNT–LCE nanocomposite film, while the contraction stress in the blank LCE film was almost 0. The SWCNTs can efficiently absorb and convert photoenergy into thermal energy, thus acting as nanoscale heaters uniformly embedded in the LCE matrix. SWCNTs also have high thermal conductivities. Moreover, previous research work showed that SWCNTs can form a percolation network in polymer matrices at loading levels above 0.1 wt%.<sup>23</sup> Thus, at such loading levels of SWCNTs, SWCNTs can serve as effective thermal conduction pathways to heat the LCE matrix uniformly and rapidly. The absorbed thermal energy increased the temperature in the

material to above  $T_{ni}$ , leading to the nematic–isotropic phase transition and axial strain in the LCE nanocomposite.

The IR-induced actuation characteristics of the LCE and SWCNT–LCE nanocomposites were also measured. Experimental results showed that when the IR irradiation was  $1.7\text{ W cm}^{-2}$ , there was almost no contraction stress in the blank LCE film, while the contraction stress in the SWCNT–LCE nanocomposite film with an SWCNT content of 0.3 wt% was 55 kPa. When the IR irradiation was  $3.4\text{ W cm}^{-2}$ , the contraction stress in the blank LCE film was 14 kPa, while the contraction stress in the SWCNT–LCE nanocomposite film was 80 kPa. This indicates that both the blank LCE and the SWCNT–LCE nanocomposites can be actuated by IR irradiation since IR is a strong thermal radiation source compared to the general visible light sources, including white light. However, in the SWCNT–LCE nanocomposites, the SWCNTs can efficiently absorb the irradiation and convert it into thermal energy to heat up the LCE matrix; therefore, the needed IR irradiation intensity to actuate the blank LCE is much higher than that to actuate the SWCNT–LCE nanocomposites.

The maximum axial contraction ratio, which is the axial contraction strain between  $T_{ni}$  and the room temperature, under photoirradiation for each sample is also listed in Table 1. All of the SWCNT–LCE nanocomposite samples were fully contracted under white light, while the blank LCE was actuated by IR light. The maximum axial contraction ratio of the blank LCE is about  $1/3$ . The SWCNT–LCE nanocomposites with different SWCNT contents show similar maximum axial contraction ratios to the blank LCE, indicating that the addition of SWCNTs into LCE matrix did not attenuate the actuation.

Fig. 7 shows the temperature change of the blank LCE and SWCNT–LCE nanocomposite films under the irradiation of the white light. After the irradiation started, the temperature at the surface of the SWCNT–LCE nanocomposite film could rise from room temperature to about  $80^\circ\text{C}$ , which is above its  $T_{ni}$ , within 10 seconds, and eventually reached  $90^\circ\text{C}$ . When the light source was switched off, its temperature dropped from  $90^\circ\text{C}$  to near  $50^\circ\text{C}$ , which is obviously below its  $T_{ni}$ , within 10 seconds. In contrast, the temperature at the surface of the blank film could

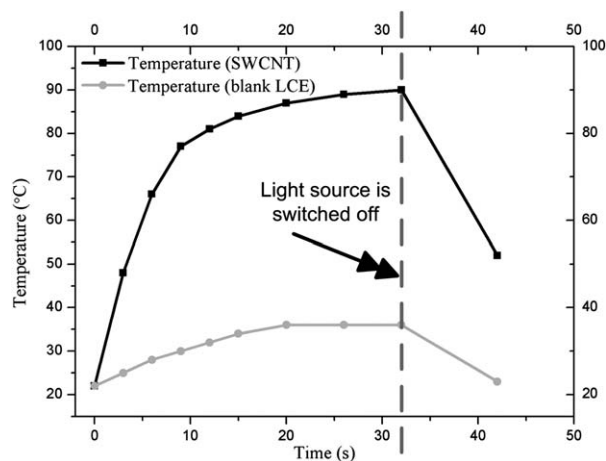


**Fig. 7** Change in temperature of the blank LCE film and the SWCNT–LCE nanocomposite film (SWCNT content: 0.3 wt%) under the white light stimulus. The irradiation intensity is  $230\text{ mW cm}^{-2}$ .

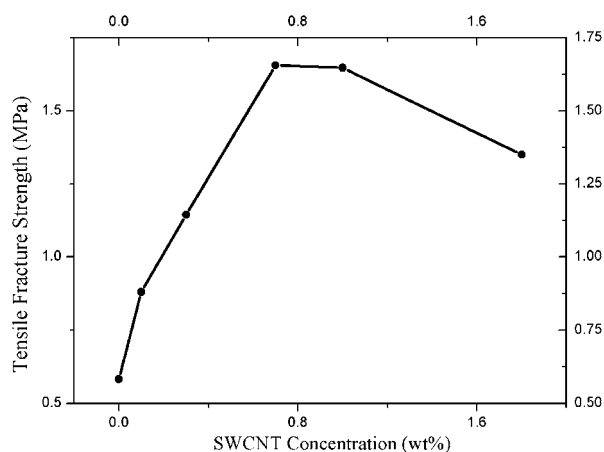


**Fig. 8** Plot of the tensile fracture strength of the SWCNT-LCE nanocomposites vs. the SWCNT content.

only rise to 36 °C, which is far below its  $T_{ni}$ , under the irradiation of the white light.

In addition, experiments indicated that some mechanical properties of the SWCNT-LCE nanocomposites were improved due to reinforcement from the SWCNTs. The tensile fracture strength of the SWCNT-LCE nanocomposites is significantly higher than that of the blank LCE, as shown in Fig. 8.

## Conclusions

Among various materials used in actuator designs, the nematic LCEs would be of especial importance due to their large deformation, reversible actuation, relative ease to manipulate and control, *etc.* The study of photoactuation of LCE materials shows that nematic LCEs have a great potential in practical applications, including artificial muscles, micro- and nano-actuators, and micro-robots.<sup>8–11</sup> In our work, the nanocomposite films of SWCNT-LCE with polysiloxane backbone and pre-aligned side-on mesogenic units were successfully prepared *via* a two-stage crosslinking process coupled with a drawing technique. High level of SWCNTs can be loaded and effectively dispersed into the LCE matrix in this simple process, and relatively thick films can be fabricated. Some salient characteristics were observed: the SWCNT-LCE nanocomposites can not only be actuated by IR light as previously reported, but also by much wider spectrum of light with an intensity on the order of 100 mW cm<sup>-2</sup>;  $T_{ni}$  of SWCNT-LCE nanocomposites are significantly lowered from that of the blank LCE as compared to previously reported; the maximum contraction was not attenuated by SWCNTs filled in the LCE matrix. Much wider choice of light source for actuation and much lower required actuation temperature (due to much lower  $T_{ni}$ ) of our SWCNT-LCE nanocomposites significantly increase the practicality of the applications of the nematic LCE materials. Filling SWCNTs in LCE matrix can also help improve the mechanical properties, which also enhances the practicability of the materials. In the

future, we will study the effects of SWCNTs on the mechanical properties of the LCE nanocomposites and their potential applications in micro-mechanical systems. The mechanism of lowering of  $T_{ni}$  with incorporated CNTs will also be further investigated.

## Acknowledgements

This work was mainly supported by Wisconsin Institutes for Discovery and was partly supported by U.S. National Science Foundation under Grant ECCS 0702095. This research utilized NSF-supported shared facilities at the University of Wisconsin. The authors thank Prof. N. L. Abbott, Dr Z. Q. Yang and members of MNSA Research Lab for technical communications, and the Materials Science Center of The University of Wisconsin-Madison for assistance in SEM and DSC measurements.

## Notes and references

- 1 J. E. Huber, N. A. Fleck and M. F. Ashby, *Proc. R. Soc. London, Ser. A*, 1997, **453**, 2185–2205.
- 2 K. Bhattacharya, *Microstructure of Martensite*, Oxford University Press, Oxford, 2004.
- 3 A. Lendlein, A. M. Schmidt and R. Langer, *Proc. Natl. Acad. Sci. U. S. A.*, 2001, **98**, 842–847.
- 4 M. Warner and E. M. Terentjev, *Liquid Crystal Elastomers*, Oxford University Press, Oxford, 2003.
- 5 J. Kupfer and H. Finkelmann, *Makromol. Chem. Rapid Commun.*, 1991, **12**, 717–726.
- 6 H. Finkelmann, E. Nishikawa, G. G. Pereira and M. Warner, *Phys. Rev. Lett.*, 2001, **87**, 015501.
- 7 Y. L. Yu, M. Nakano and T. Ikeda, *Nature*, 2003, **425**, 145.
- 8 M. Camacho-Lopez, H. Finkelmann, P. Palfy-Muhoray and M. Shelley, *Nat. Mater.*, 2004, **3**, 307–310.
- 9 M. Yamada, M. Kondo, J. I. Mamiya, Y. L. Yu, M. Kinoshita, C. Barrett and T. Ikeda, *Angew. Chem., Int. Ed.*, 2008, **47**, 4986–4988.
- 10 S. Xu, H. W. Ren, Y. J. Lin, M. G. J. Moharam, S. T. Wu and N. Tabiryan, *Opt. Express*, 2009, **17**, 17590–17595.
- 11 F. T. Cheng, R. Y. Yin, Y. Y. Zhang, C. C. Yen and Y. L. Yu, *Soft Matter*, 2010, **6**, 3447–3449.
- 12 S. Iijima, *Nature*, 1991, **354**, 56–58.
- 13 S. N. Kim, J. F. Rusling and F. Papadimitrakopoulos, *Adv. Mater.*, 2007, **19**, 3214–3228.
- 14 W. Y. Zhou, X. D. Bai, E. G. Wang and S. S. Xie, *Adv. Mater.*, 2009, **21**, 4565–4583.
- 15 M. A. Hamon, M. E. Itkis, S. Niyogi, T. Alvarez, C. Kuper, M. Menon and R. C. Haddon, *J. Am. Chem. Soc.*, 2001, **123**, 11292–11293.
- 16 H. Koerner, G. Price, N. A. Pearce, M. Alexander and R. A. Vaia, *Nat. Mater.*, 2004, **3**, 115–120.
- 17 L. Q. Yang, K. Setyowati, A. Li, S. Q. Gong and J. Chen, *Adv. Mater.*, 2008, **20**, 2271–2275.
- 18 Y. Ji, Y. Y. Huang, R. Rungsawang and E. M. Terentjev, *Adv. Mater.*, 2010, **22**, 3436–3440.
- 19 S. V. Arehart and C. Pugh, *J. Am. Chem. Soc.*, 1997, **119**, 3027–3037.
- 20 O. Mitsunobu, *Synthesis*, 1981, **1**, 1–28.
- 21 K. K. Hon, D. Corbett and E. M. Terentjev, *Eur. Phys. J. E*, 2008, **25**, 83–89.
- 22 S. V. Ahir and E. M. Terentjev, *Nat. Mater.*, 2005, **4**, 491–495.
- 23 R. Ramasubramaniam, J. Chen and H. Liu, *Appl. Phys. Lett.*, 2003, **83**, 2928–2930.
- 24 Experiments indicated that if the ends of the films were free and not loaded, the maximum axial contraction ratios would be a little smaller compared to when the ends of the films were loaded.